Journal of Electronic Materials, Vol. 13, No. 2, 1984

JUNCTION SOLAR CELLS MADE WITH MOLECULAR BEAM GLOW DISCHARGE BOMBARDMENT

E.J. Caine[†] and E.J. Charlson

Electrical Engineering Department
University of Missouri-Columbia
Columbia, Missouri 65211

(Received July 18, 1983)

The fabrication and characterization of silicon p-n junction solar cells with various glow discharge, unanalyzed, molecular implanted emitter regions is described. Total area simulated air mass one (AM1) power conversion efficiencies without AR coatings or back surface fields are at best 8.2% compared to 9.1% for conventionally implanted or $POCl_3$ thermally diffused cells on similar substrates. To achieve optimum performance, Q-switched ruby laser light was incorporated into the molecular implant annealing procedure. Conversion efficiencies greater than 8% were achieved with the four dopants BCl_3, PCl_3, AsF_3 and $POCl_3$. For similar processing, conversion efficiency with BF_3 implants was less than those of previous investigations, most likely due to poor crystalline regrowth of the heavily doped emitter regions. Cell quantum efficiency and mesa junction ideality are shown to be similar to those of con-

---

† Now at Santa Barbara Research Center, Goleta, CA 93117. Work submitted in partial fulfillment of Ph.D. in Electrical Engineering at the Univ. of Missouri, Columbia, MO 65211

ventional cells while molecular implant sheet resistance values varied, generally being directly related to the dopant molecular weight.

Key words: Silicon solar cells, ion implantation, glow discharge, laser annealing, beam processing

Introduction

With the application of ion implantation and pulsed laser annealing techniques to the fabrication of silicon solar cells, power conversion efficiences have become comparable to p-n junction devices made with conventional thermal diffusion or with ion implantation followed by multi-step furnace annealing (1-3). Several advantages make the ion implanted/laser annealed approach attractive: high electrical activation of dopant atoms with the ability to exceed thermal equilibrium solid solubility limits (4-5), preservation of bulk (substrate) minority carrier diffusion length (5), dopant profile tailoring (5-6) and superior implant layer recrystallization over that of thermal furnace anneals (7).

There are, however, several limitations to the use of conventional implanters for large scale production of silicon solar cell devices. These include the initial cost of equipment, operation complexity and limited maximum dosage capability.

It has been found that, in general, silicon layers implanted with BF_2^+ as opposed to B^+ (with equivalent dosages and target impact velocities), have resulted in superior junctions in terms of greater dopant activation, superior crystallinity and junction leakage (8-10). The greater usable percentage of BF_2^+ from a BF_3 ion source has led to lower obtainable critical (amorphous) dosage conditions (11). Others (11-12) have suggested using similar molecular ions (eg. AsF_2^+ or As_2^+ for As^+ which can result from arsenic containing sources) because of a larger molecular species current as compared to the atomic current. This would translate into shorter implant times, a condition desirable for solar cell manufacture.

Simple direct current glow or corona discharge apparatus have been successfully used in conjunction with the fabrication of silicon solar cells with either furnace or laser anneals (13-15). These involve unanalyzed or "dirty" implantations using BF_3 or PF_5 source gases.

This paper describes similar work using the glow discharge approach in creating silicon p-n junctions with several additional organic and inorganic source compounds. It also provides relative performance characteristics for solar cells made with each of these sources and with standard diffused and conventional ion implanted base line cells.

Experimental

Most starting material used in this investigation was Monsanto (111), 4 to 10 ohm-cm n type and 2-6 ohm-cm p type Czochralski silicon with thickness varying from 178 to 280 μm depending on the type. Some cells were also made with 432 μm material (3-6 ohm-cm n type) as will be noted. The wafers were polished on one side by the manufacturer.

Cell fabrication was divided into 3 groups: molecular glow discharge implantation, conventional implantation, and diffusion, the latter two being used for comparison purposes. Molecular implantation and diffusion were performed on material 0.71 × 0.71 cm (0.5 cm^2), the final solar cell size. Conventional implantation was performed on 5 or 7.5 cm diameter wafers which were then scribed into this same size. Substrate material was cleaned with 10% HF acid and DI rinsed, a five min. ultrasonic sequential organic clean with each of trichloroethylene, acetone, methanol and DI rinse and a five min. boil in each of HCl and HNO_3 acids, followed by hot and cold DI rinses.

Conventional ion implantation was performed on wafers similar to those used for discharge implants using a Western Electric machine (16). Implant conditions were the same for both ^{11}B and ^{31}P, namely, 2×10^{15} atoms/cm^2 dosage at 30 keV. Target wafers were held in a rotating platen to limit temperature rises.

Diffused emitter regions were formed with a standard $POCl_3$ open tube furnace technique at 855°C giving a sheet resistance of approximately 50 ohms/square. The backside, unpolished surface was lapped to remove the junction.

Glow Discharge

The glow discharge implantation reactor, seen in Fig. 1 is basically the same as that given by Wichner and Charlson (13) with some structural modifications including: a smooth cylindrical glow region, the capacity to use gases from liquid dopant vessels and improved pump capability. Implantation begins by placing the substrate in the center of the chamber cathode (with an 8 cm^2 exposed polysilicon area). With the source valve closed, the system is pumped to 5×10^{-5} Torr on the cold trap assembly. The source valve is then opened and the chamber differential pressure

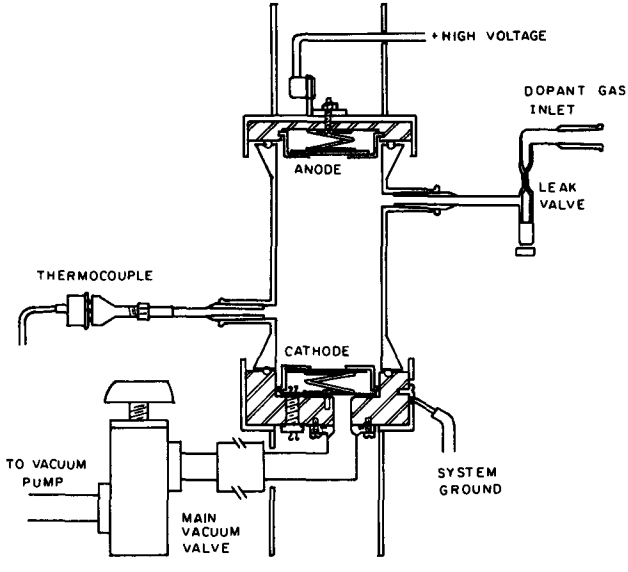

Fig. 1. Glow discharge implantation reactor.

adjusted to approximately 10 μm. The dc voltage is applied and increased while the leak valve is adjusted until the desired pressure, current and voltage conditions are obtained taking less than one minute for all implants. Discharge voltage is maintained at 4.5 to 6.0 kV with typical currents of 1 mA with 4 to 5 min. bombardment times.

The dopant sources and their molecular weights used in this study are shown in Table I. Discernable discharge colors were viewed for the various dopant gases used in this study. Also, three distinct patterns became evident, although quite dissimilar to the classical "glow" pattern (17). See Fig. 2 and Table I for the characteristic discharge pattern and color.

TABLE I

Molecular Dopant Compounds with Discharge Type and Color

Compound	Mol.Wt.	Type[a]	Color
Boron Trifluoride BF_3	67.80	A	light pinkish blue
Trimethyl Borate $B(OCH_3)_3$	103.92	A	light blue
Boron Trichloride BCl_3	117.19	C	light pinkish blue
Trimethyl Phosphite $P(OCH_3)_3$	124.08	A	reddish purple
Arsenic Trifluoride AsF_3	131.92	B	whitish blue[b]
Phosphorus Trichloride PCl_3	137.33	C	light pinkish blue
Phosphorus Oxychloride $POCl_3$	153.35	C	light orange blue
Arsenic Trichloride $AsCl_3$	181.27	C	light orange blue

a. See Fig. 2; b. Cathode region was reddish purple

The current-voltage (I-V) characteristics of the discharge chamber are given in Fig. 3 for a typical discharge in trimethyl borate at 10 mTorr and 13 mTorr. Electrode spacing was approximately 18 cm with 3 cm diameter electrically exposed electrodes. Figure 3 also shows published data for a glow discharge in argon ambient for 12.5 cm diameter electrodes spaced 6.4 cm apart (17).

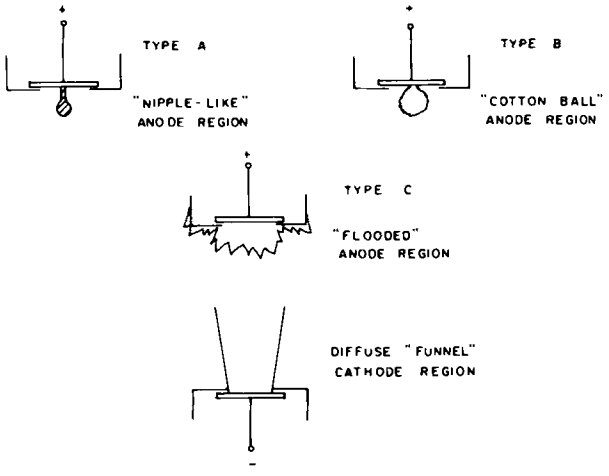

Fig. 2. Basic discharge types for molecular dopants.

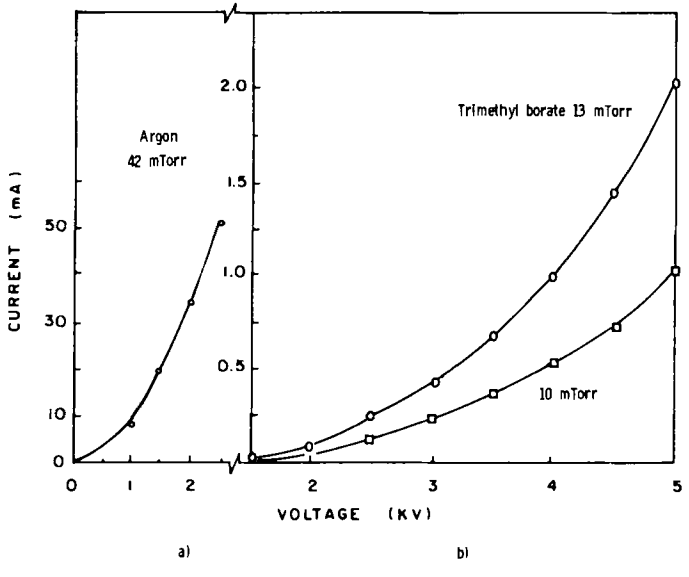

Fig. 3. Glow discharge current-voltage characteristics. (a) Normal argon discharge from Ref. 17 and (b) Implantation reactor trimethyl borate discharge.

Annealing and Contacts

Generally three basic annealing techniques were used on the implanted cell structures:

t - One or three-step thermal furnace anneals under flowing nitrogen.

1 - Q-switched ruby laser annealing performed in air with one pulse using the multimode operation. Laser energies were less than or equal to 1.5 Joules/cm^2 for a 35 nsec pulse.

1t - Combination of t and 1.

Some diffused cells also had either a laser or furnace post-diffusion anneal. Before and after annealing, samples were etched in 10% HF followed by a DI water rinse.

Both front and back ohmic contacts (6) to the cells were 7000A of filament evaporated aluminum. N-type substrates were lapped first with number 400 grit prior to metallization (unsintered) for a back contact. Back contacts on p-type substrates were sintered with a cycle of 10 min. ramp up to 400°C, 20 min. hold and 10 min. ramp down. No back surface fields or antireflection coatings were used. Edges were etched with a standard silicon etch to remove shunt damage.

Target Implantation Temperature

Target temperature rise was investigated by epoxying a 1 mil diameter chromel-alumel thermocouple (Omega Engineering) to a cell underside (18). Other approaches have utilized noncontacting infrared heat probes (19) or solving appropriate system heat equations (19-20). A knowledge of the actual temperature of the target sample is important for several reasons including: controlling the implanted electrical activity uniformity, controlling the degree of ion-induced damage and limiting target warp and decomposition.

Several factors determine the actual temperature rise during bombardment: ion beam and target dimensions, target surface emissivity, heat losses through target holder conduction and heat exchange between the target and surroundings. Using trimethyl borate as the bombarding ion, typical runs at 5 keV accelerating energy showed temperature rises from 220°C to 460°C for operating currents of 0.5 to 2.5 mA, respectively.

Results

Sheet Resistance

The emitter layer sheet resistance for the various processes will be presented in a series of two graphs. Comparative data is given first in Fig. 4 for the conventionally implanted emitters (^{11}B and ^{31}P) with a single pulse laser anneal or a 1-step 30 minute thermal anneal. A sharp reduction in sheet resistance is seen for ^{11}B implants for laser energy densities greater than 1.0 J/cm^2. At 1.5 J/cm^2 values of sheet resistance were comparable to those obtained for 1000°C thermal treatments and this energy density was used as a standard for all other anneals in this investigation. Data from Beanland (8) for a one step thermal anneal of ^{11}B are also given for comparison.

Figure 5 shows data for 30 minute 1-step thermally annealed silicon implanted in the glow discharge system with BF_3 and PCl_3 for two different reactor implant conditions of current, voltage, and time. The primary result seen is that an increased reactor current-time product does not significantly increase layer conductivity for similar anneals. Conventional implantation results with BF_2^+ (22) in Fig. 5 shows significant variations with anneal temperatures as with our data but also show the effects of variation of dosage. It should be pointed out for simplicity no attempts were made to correct the target current for effects such as secondary electron emission, so that true implant currents may differ somewhat from values reported here. Also sputtering of the target surfaces may limit the maximum dopant dosage (23-25).

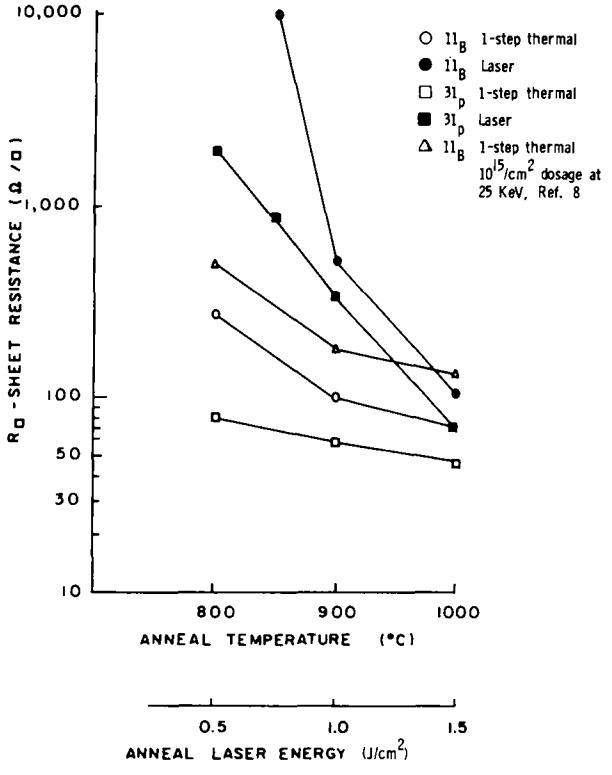

Fig. 4. Conventional implanted emitter sheet resistivity as a function of laser energy density and 1-step thermal anneal. Dose for this study was $2\times10^{15}/cm^2$ at 30 keV.

Table II shows representative emitter layer sheet resistances of molecular implanted cells. The following inferences may be made:

a) Sheet resistances ranged from 31 to 180 ohms per square.

b) Above a molecular weight 117.19 the sheet resistance tends to increase with molecular weight. Results of SIMS data, to be presented later, indicate dopant segregation at the surface for

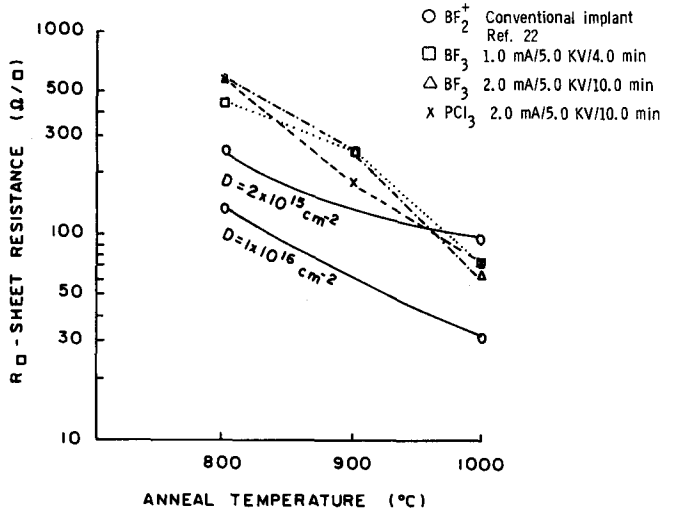

Fig. 5. Molecular implanted emitter sheet resistance as a function of 1-step thermal anneal.

both BF_3 and $B(OCH_3)_3$. The resultant reduction in surface carrier mobility could account for the tendency for these two sources to produce emitters with high sheet resistance, although BF_3 is small to begin with.

c) The post laser anneal did not consistently reduce sheet resistance.

d) The increase in beam current-time product in some instances did not decrease the sheet resistance.

The cells used in this study were relatively small (0.7×0.7 cm) compared to commercial cells. In order to implant larger area cells it is important to know the variation in implant concentration across the implant target (cathode). To investigate this, "strip cells" of dimension 0.7×3.1 cm were implanted. By uniformly annealing these strips one can obtain a rough estimate of the beam current density as a function of cathode location and an idea of

TABLE II
Emitter Sheet Resistance of
Molecular Implanted Silicon Solar Cells

Dopant (MW)	Cell	Implant Conditions[a]	Anneal[b]	Sheet R (ohm/sq)	Species Avg (ohm/sq)
BF_3 (67.8)	214A	1/5/4	l	100	55.75
	214B	1/5/4	lt	45	
	216A	2/5/10	l	46	
	216B	2/5/10	lt	32	
$B(OCH_3)_3$ (103.9)	186	1/5/4	l	115	120
	200	2/5/10	l	125	
BCl_3 (117.19)	117	1/6/15	l	45	38
	122	1.3/5.8/15	lt	31	
$P(OCH_3)_3$ (123.9)	107	1/6/10	l	48	71.5
	109	1.5/6/15	lt	95	
AsF_3 (131.9)	162	1/5/2.5	l	70	80
	170	1.8/5.3/16	l	77	
	161	1.1/4/5	lt	93	
PCl_3 (137.3)	208	1/5/4	l	120	116
	203	1/5/4	lt	115	
	209	2/5/10	lt	114	
$POCl_3$ (153.3)	99	1.6/6/15	l	120	115
	98	1.6/6/15	lt	110	
$AsCl_3$ (181.27)	173	1.2/5/10	l	135	157
	181	1.9/5.6/10	l	180	

a. Current (ma)/Voltage (kV)/Time (min).
b. l-laser at 1.4-1.5 J/cm^2; lt-laser and thermal 700°C-20 min.

the radial doping uniformity from the variation of sheet resistance along the strip.

Figure 6 gives the results of 3 mm spaced 4-point probings on 6 strip cells with 2 extreme bombardment conditions for each of three dopants, boron trifluoride, trimethyl borate and phosphorus trichloride. Generally there is symmetry in the data about the 15 mm center reference point. The two PCl_3 strips exhibited a dip at 9 mm, most likely due to contamination of the cathode surface noticed near this position. The PCl_3 strip with the smallest current time product also showed some evidence of a sheet resistance peak around 15 mm. This could possibly be due to sputter erosion. Oddly for this dopant the strip with the larger current-time produce exhibited overall a higher sheet resistance.

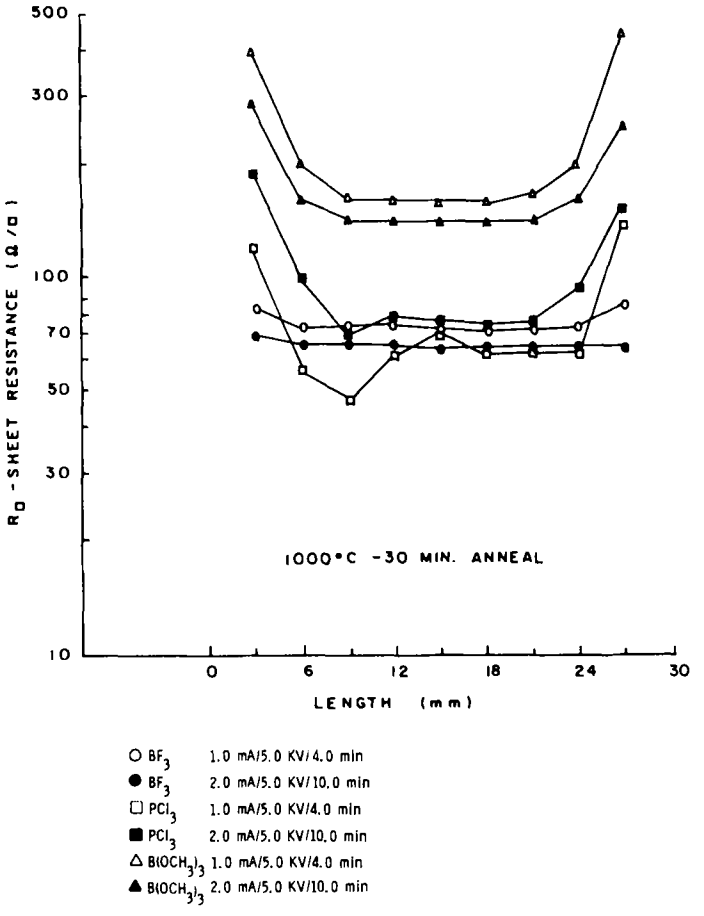

Fig. 6. Strip cell sheet resistance profile for various implanted molecular dopants, annealed at 1000°C with a 1-step anneal.

Edge effects (distortions in current flow) will account for some increased reading at the strip ends, (as seen from the sheet resistance probing). In order to estimate the extent of this effect for a worst case reading 3 mm from the strip end, a square-shaped cell could be assumed 6 mm on a side with the probe positioned in the

center. In this case the sheet resistance would be 86% of the measured value (26).

Significant surface erosion in the form of a "dimple" was evident on molecular implanted cells for all dopants except trimethyl borate and trimethyl phosphite. Figure 7 shows a surface profilometer trace for one extreme case evidenced by a $POCl_3$ implantation. It is possible that the absence of the dimple for trimethyl borate and trimethyl posphite is due to the lack of chlorine or fluorine in these compounds compared to the other dopant sources.

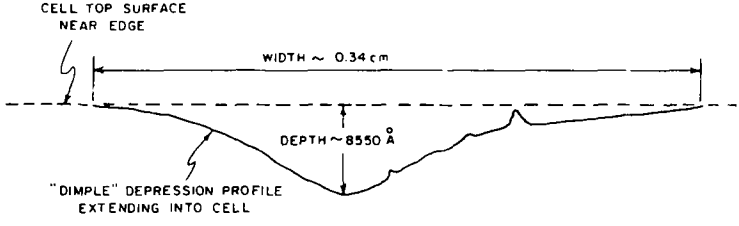

Fig. 7. Sputter depression, "dimple," for glow discharge implanted phosphorus oxychloride cell #98.

All laser annealed (> 0.5 J/cm^2) implanted surfaces exhibited to some degree rippling in the form of concentric rings with a periodicity of 35-50 μm. This wavelength is much larger than that reported by others, 1 μm (27) and 4.52 μm (28), for Nd-YAG and ruby lasers, respectively. Unfortunately, no criterion could be established as to their significance indicative of successful implant layer annealing.

The resulting laser-induced pattern for trimethyl borate was more complicated than previously noted in that cellular formation was evident. See Fig. 8. It is speculated that the dark lines are the result of laterally segregated implant dopant. This is suggested by the striking resemblance to transmission electron micrographs of laser treated indium implanted silicon published by Narayan (29). Two different mechanisms (30) have been suggested for cell formation, depending on the cell size: supercooled melt solidification - 0.1 μm diameter or cellular convection - 1.0 μm diameter.

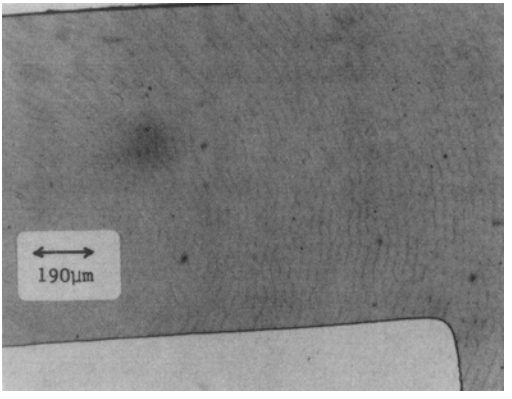

Fig. 8. Laser induced surface rippling for a trimethyl borate implanted cell.

SIMS Measurements

Secondary ion mass spectroscopy (SIMS) measurements were performed on several cells with boron doped emitter regions using a Cameca IMS 3F ion microscope with an O_2^+ 15 keV primary beam. The ultimate sensitivity of this system is $5\times10^{14}/cm^3$. Profiles are shown in Figs. 9 and 10.

The annealed dopant profiles for ^{11}B and BCl_3 are typical and generally follow a Gaussian type distribution. The shorter range for the BCl_3 and $B(OCH_3)_3$ is due to the lower accelerating voltage present with the discharge system (~5 kV). In the case of trimethyl borate there appears to be considerable segregation of the boron at the surface. A more extreme case of dopant segregation was found on BF_3 emitters with a thermal one step anneal and is shown in Fig. 10. Also shown in the same figure is a laser annealed BF_3 sample where the segregation has been eliminated by a single laser pulse. It should be noted, however, that there are large dopant densities concentrated at the surface associated with BF_3/laser combination leading to the possibility of large surface recombination. Indeed, solar cells using BF_3 implanted emitters were found to have

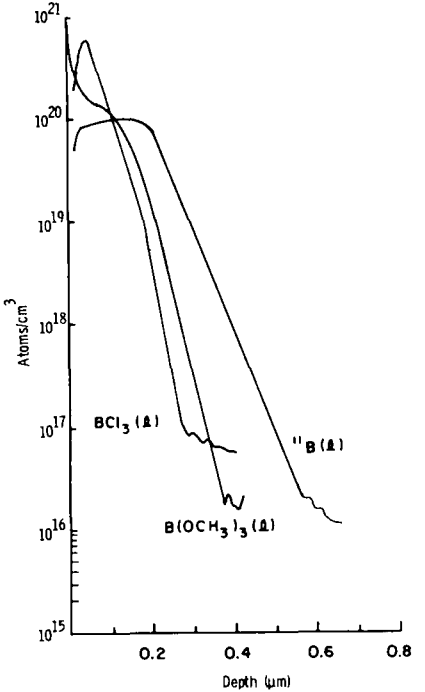

Fig. 9. SIMS profiles for various implanted and annealed dopants.

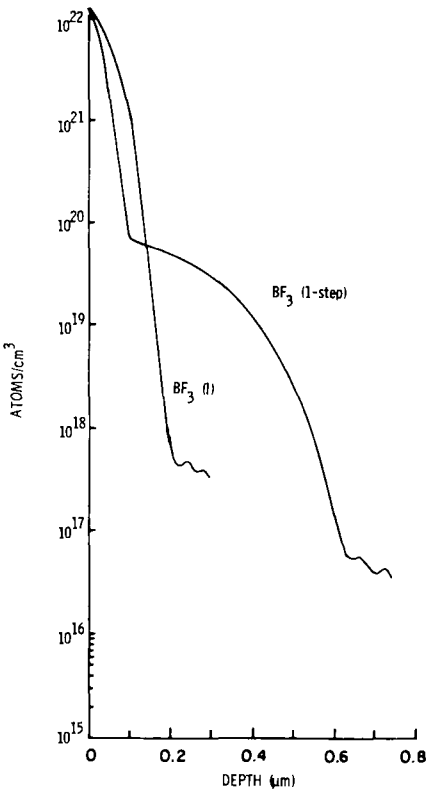

Fig. 10. SIMS profiles for BF_3 glow discharge implanted and annealed cells.

inferior short circuit currents, approximately 10% less than other molecular cells.

Rostron (31) has theoretically predicted the contribution of the emitter region of a typical n/p silicon solar cell under AMO conditions and found it to be at most 13% of the total short circuit current.

It is postulated that our reduced current is due to excessive carrier recombination due to lattice strain and defects created by the high dosage BF_3 bombardment and subsequent epitaxial regrowth. Fig. 11 supports this supposition by showing a network of linear etch features in the three <110> directions, perhaps being the intersection of numerous stacking faults on the three {111} facets intersecting the (111) silicon surface. Fisher and Amick (32) have reported seeing similar etch features identified as stacking faults attributed to the oxidation of damaged silicon surfaces. The delineation etch in our case was the standard silicon etch of 4 parts HNO_3 and 1 part HF. This etch in addition was used as an edge etch on all cells in this investigation, however, only the BF_3/laser cells showed the marked dislocation pattern.

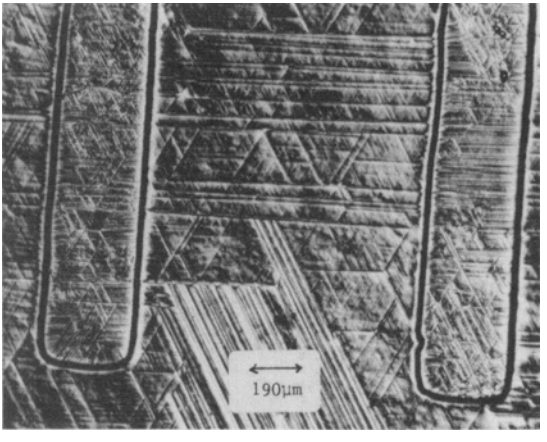

Fig. 11. Photograph of the surface of a BF_3 cell after delineating etch showing large number of stacking fault lines.

It was also observed that after laser annealing all BF_3 cells exhibited a sky-blue surface color, unlike other implants where the surface was metallic gray. This effect was unique to laser annealed cells. Thermal post laser annealing changed the surface color somewhat but not totally back to the normal metallic gray.

Solar Cell Performance

Over the period of this study, approximately 175 solar cells were fabricated into working devices, 100 of these having molecular implanted emitters. The remaining devices were fabricated with conventional techniques of open tube diffusion and ion implantation to serve as a baseline for performance comparison.

Standard electrical parameters (open circuit voltage E_{oc}, short circuit current density J_{sc} and AM1 power conversion efficiency η) will be given first for the baseline cells. The tungsten filament solar cell simulator was calibrated with a standard cell from Lawrence Livermore Laboratory and cross checked at Oak Ridge National Laboratory. Table III gives best cell performance data grouped according to either Q-switched ruby laser (1) or furnace thermal (t) annealing.

TABLE III

Electrical Characteristics of Base Line Cells

	Laser					Thermal				
Species	Cell[a]	E_{oc}(V)	J_{sc}(mA/cm^2)	FF	η (%)	Cell	E_{oc}(V)	J_{sc}(mA/cm^2)	FF	η (%)
				Implanted						
P	50 1t	0.559	20.78	0.747	8.66	55	0.556	21.7	0.74	9.00
B	39 1t	0.54	21.20	0.706	8.13	31	0.517	18.0	0.70	6.52
				Diffused						
$POCl_3$	8 1	0.56	21.8	0.740	9.08	2	0.555	22.17	0.736	9.06

a. 1 - laser; 1t - laser-thermal

It should be noted that simple processing steps were chosen for device fabrication, i.e. no AR coating, no back-surface fields and a three finger (10% coverage) top grid contact. Single layer AR coatings typically increase efficiency by 35%. Specific device instances will be noted, though, that show the enhanced short circuit current due to thicker substrates (optimally 432 μm (33)) and improved fill factor due to a 12 finger (10% coverage) top grid collection contact.

Baseline Cells

Thermal annealing alone gave the best results for those devices with phosphorus implants if the 3-step procedure (2) was used (Cell 55). This involved 550°C/90 min-850°C/15 min-550°C/90 min. Single step anneals were not as successful due to conflicting anneal characteristics of emitter dopant activation and degrading substrate carrier diffusion lengths.

Annealing with the laser had to be augumented with a 700°C/20 min. furnace step (34) to achieve the optimum performance as shown in cell 50. A 9% efficiency increase was due to a 25-30 mV increase in E_{oc}, compared to a cell with laser annealing alone.

Cells with boron implants gave identical best results for either a 1-step (cell 31 [950°C]) or 3-step furnace thermal anneal but had an approximate 24% degraded efficiency below that with combination laser/thermal anneals. Again the benefit of the post-laser heat treatment was evident with a 60-70 mV increase in E_{oc}. A 400°C/20 min. pre-laser anneal (35) showed no improvement in cell performance, as with phosphorus, indicating that if implant channeling damage were annealed, its affect was negligible. Also the lower E_{oc} for the boron implants is most likely due to lower peak dopant concentration as predicted by LSS theory (36).

The $POCl_3$ diffused cells gave nearly identical results to the best phosphorus implanted devices irrespective of the post-diffusion treatment given. A laser treatment reduced emitter sheet resistance from 50 to 38 ohms/square indicating higher phosphorus dopant activation and/or precipitate removal (37).

Molecular Cells

In discussing the performance of solar cells made with glow discharge implants, it seems appropriate to first make some general comments about all cells generally as compared to cells made with conventional techniques. Comparison will then be made between and among cells of each type (See Tables IVa and IVb).

As already discussed, the largest AM1 conversion efficiency for both conventional implantation and diffusion formed junction cells was 9.1%. This efficiency was characteristic of both $^{31}_{11}P$ implanted and $POCl_3$ diffused emitters. The best ^{11}B implanted cells had an efficiency of 8.1%. Under identical test conditions and with post-implantation device processing, 8.2% efficiency was the highest seen for molecular implants. This varied from 6.1% for trimethyl borate to 8.2% for phosphorus oxychloride. Four molecular dopants gave efficiencies greater than 8% (all with laser processing): $POCl_3$ - 8.2%, PCl_3 - 8.1%, BCl_3 - 8.1% and AsF_3 - 8.05%. In general both lower fill factor and open circuit voltages were the primary cell performance factors that limited the devices. The boron trifluoride group was the only exception due to short circuit current limitations, previously discussed. Excluding this latter group, E_{oc}'s were at most 0.542V with 0.73 the maximum fill factor. For the best ^{31}P implanted cells on identical substrates, the maximum E_{oc} and fill factor were 0.56V and 0.747, respectively. Phosphorus oxychloride diffused cells were similar.

Thermal annealing produced glow discharge cells with efficiencies between 5.3% and 8.1%, the latter being for 3-step annealed $POCl_3$. This scheme was effective in giving high open circuit voltages (0.55V) and short circuit currents (21 mA/cm^2), but low fill factors (0.62 - 0.68), most likely due to low dopant activation as a result of the relatively higher molecular induced crystalline damage.

Table IV gives the best cells performance data for molecular implanted emitters along with implant conditions. The dopant types are listed with increasing molecular weight.

TABLE IVa
Electrical Characteristics of
Molecular Implanted Silicon Solar Cells

		Laser[a]				
Species	Cell	E_{oc}(V)	J_{sc}(mA/cm^2)	FF	η (%)	Implant Conditions[b]
BF_3	215A	0.512	15.24	0.724	5.65	2.0/5.0/10
	215B[c]	0.544	19.18	0.738	7.66	2.0/5.0/10
	216B[c,d]	0.558	20.71	0.720	8.35	2.0/5.0/10
$B(OCH_3)_3$	190	0.495	21.0	0.59	6.10	2.0/5.0/10
	200[d]	0.513	23.34	0.61	7.34	2.0/5.0/10
BCl_3	116	0.537	20.58	0.73	8.09	1.5/6.0/10
$P(OCH_3)_3$	111	0.52	20.24	0.68	7.2	1.2/6.0/15
AsF_3	157	0.53	21.31	0.71	8.05	1.0/5.5/10
PCl_3	212	0.525	21.44	0.72	8.1	2.0/5.0/10
$POCl_3$	101	0.534	22.0	0.70	8.23	1.0/6.0/10
$AsCl_3$	173	0.50	21.13	0.67	7.16	1.2/5.0/10

a. Laser energy 1.5 J/cm^2
b. Current (mA)/Voltage (kV)/Time (min)
c. Laser-thermal anneal 1.5 J/cm^2-700°C/20 min.
d. 432 μm thick substrate

TABLE IVb
Electrical Characteristics of
Molecular Implanted Silicon Solar Cells

		Thermal					
Species	Cell	E_{oc}(V)	J_{sc}(mA/cm^2)	FF	η (%)	Implant Conditions[a]	Anneal
BF_3	147	0.51	17.9	0.727	6.6	1.9/5.7/10	1-step 1000°C
$B(OCH_3)_3$	189	0.51	18.8	0.55	5.3	1.0/5.0/4	1-step 1000°C
BCl_3	123	0.525	20.67	0.59	6.38	1.7/5.5/15	3-step 850°C
$P(OCH_3)_3$	104	0.522	16.38	0.75	6.33	0.9/6.0/15	1-step 1000°C
AsF_3	169	0.532	20.76	0.7	7.64	1.0/5.1/5	3-step 850°C
PCl_3	211	0.552	21.03	0.66	7.66	2.0/5.0/10	3-step 850°C
$POCl_3$	93	0.55	20.87	0.64	7.26	1.0/6.0/15	3-step 850°C
	93[b]	0.554	20.57	0.73	8.27		
	95	0.557	21.74	0.68	8.1	1.0/6.0/15	3-step 900°C
$AsCl_3$	178	0.53	19.72	0.51	5.3	1.5/5.7/3	3-step 850°C

a. Current (mA)/Voltage (kV)/Time (min)
b. 12 finger metal grid

Boron Trifluoride

The laser annealing behavior of BF_3 is anomalous with respect to the other dopants used in this study. Optimum annealing was achieved only after a medium temperature heat treatment (700°C/20 min.) was incorporated after the laser anneal. Cells 215A and 215B illustrate the effect of a post-laser anneal on the short circuit current for this type cell. While the increase is good, it still is not as large as in the case of conventional cells. A second clue to this incomplete annealing was emitter surface colors. After implantation with BF_3 the surface of the cell exhibited a gold color, indicating a highly damaged layer (38). After annealing with one laser pulse this color changed to a light blue. The post-laser anneal practically eliminated this color and returned the surface to the normal dull metallic. It should be noted that no surface color was apparent after any of the thermal anneal techniques. This color transition to light blue which was seen in ^{31}P implanted cells annealed at approximately 0.9 J/cm^2 has been discussed by Beanland et al. (38). A probable explanation for it would appear to be that the total depth of the implant damage has not recrystallized to the top surface after the laser irradiation and that an extremely shallow amorphous region remains. The increase in both the short circuit current and open circuit voltage after the additional heat treatment would indicate greater activation of the emitter dopant regions (also seen in Table II), reduction in damage induced junction trapping sites and/or lower emitter surface recombination velocity.

Using a silicon substrate of 432 μm thickness (216B) produced an 8% increase of short circuit current. Separate experiments with 432 μm substrates thinned to 254 μm have shown that of this increase approximately 39% is due to longer minority carrier diffusion length (MCDL) and not greater photon absorption.

Thermal annealing alone of BF_3 cells did not prove to be as effective as that achieved with laser/thermal combination or laser annealing by itself. A 1-step furnace anneal at 1000°C produced good fill factors but had a reduced short circuit current as seen with the conventional boron and phosphorus implants. One possible explanation of this could be due to reduced bulk lifetime effects (5).

Annealing at 900°C was not tried because of increases in emitter sheet resistances. Three step annealing proved to be ineffective even with the presence of what are believed to be highly damaged emitter regions.

Trimethyl Borate

Power efficiencies were only fair in comparison to that of BF_3, the primary performance deficiency was in fill factor, indicating a larger cell series resistance and/or junction effects. (Sheet resistances measured were greater than 100 ohms/sq.) Short circuit currents were noticeably better than that of BF_3, being typically 21 mA/cm^2 for 254 μm substrate thickness and 23 mA/cm^2 for 432 μm substrate thickness. One can speculate that unannealed radiation damage near the junction or a lower peak emitter dopant concentration lowered the open circuit voltage and fill factor. Thermal annealing was less effective in all respects.

Boron Trichloride

BCl_3 gave the best boron classified cells in this investigation. The best cell performance due to laser annealing was practically identical to that realized with conventional boron implants, or about 8.1% conversion efficiency. The post-laser thermal treatment of 700°C for 20 min. enhanced the E_{oc} without affecting J_{sc} in contrast to BF_3. This would lead one to believe that initially more optimum junction space charge region and emitter layer conditions were obtained.

Thermal annealed cell performance is similar to BF_3. The emitter sheet resistance obtained for 3-step techniques was again too large for simple metal grid patterns (>350 ohms/sq.).

Trimethyl Phosphite

Of the three molecular dopants containing phosphorus used in this study, trimethyl phosphite was the least suc-

cessful in terms of power efficiencies. Laser annealed cells were hampered by poor FF's, less than or equal to 0.68. This poor performance was also seen with trimethyl borate, a similar organic compound. The presence of carbon may have seriously reduced emitter mobility. In contrast to other phosphorus dopants, 3-step anneals were ineffective in terms of producing an enhanced E_{oc} (> 0.55V), while maintaining maximum J_{sc} for a given silicon substrate. Low emitter layer conductivity did not appear to cause this problem with sheet resistances < 100 ohms/square.

Arsenic Trifluoride

The annealing characteristics and resulting cell performance of arsenic trifluoride proved to be not unlike that of boron trichloride. For laser annealing techniques, the maximum power efficiency for both was 8.1, maximum open circuit voltage was between 0.53 and 0.54 V, maximum fill factors were greater than 0.7 and short circuit current densities were among the highest seen for any cell made in this study with an average value of 21.0 mA/cm^2. Emitter sheet resistances due to laser annealing were approximately 70-80 ohms/sq., almost twice that of BF_3 or BCl_3. Because no conventional arsenic implantations were used to form solar cells, no comparisons can be made as were done for ^{11}B and ^{31}P. However, it has been observed that higher temperatures for one-step anneals are needed to obtain efficiencies with ^{75}As implants comparable to cells with boron or phosphorus implants (3).

As with BF_3, the 400°C pre-laser heat treatment produced no noticeable improvement in cell performance, again based on one cell. The use of the 700°C post-laser anneal was inconclusive, causing the emitter sheet resistance to be larger than without the treatment (93 ohms/sq. for cell #161).

Three-step thermal anneal techniques suffered from poor fill factors unless a fine grid emitter contact was used. With this latter metallization, a fill factor of 0.7 was obtained for cell #169. Previous to this, 0.59 was the highest fill factor obtained on 3-step thermally annealed

cells with the standard 3 finger comb grid pattern (BCl_3 cell #123).

Phosphorus Trichloride

Phosphorus trichloride, the second of three phosphorus-containing molecular dopant species, gave the best overall cell performance of these dopant groups. The largest power efficiencies were between 8.0 and 8.1%, these being laser annealed. A 700°C post-laser anneal increased E_{oc} 10 to 20 mV.

Three-step thermal annealing produced cells with open circuit voltages of at least 0.55 V (10 mV less than that for conventional ^{31}P implants). J_{sc}'s were of comparable value. Poor fill factors were primarily the result of lower emitter conductivity.

Phosphorus Oxychloride

The performance of these cells was identical to that of phosphorus trichloride except for the cell degradation seen with the 700°C/20 min. thermal annealing after laser treatment. For two cells with this treatment the open circuit voltage fell to an average of 400 mV, some 134 mV below the maximum voltage seen. No explanation can be offered for the effect. Emitter sheet resistances for laser annealing with or without a post-laser heat treatment were typically 115 ohm/sq.

Three-step annealing again showed the potentially large open circuit voltages possible (approximately 0.55 V), not yet realized with laser techniques. Cell 93 shows the influence on cell efficiency for 3-step annealing that the emitter fine grid metallization has, primarily increasing the fill factor from 0.64 to 0.726. Increasing the middle step temperature of a 3-step anneal to 900°C gave an improved fill factor of 0.68 for the standard grid on cell #95.

Arsenic Trichloride

Open circuit voltages were generally below 0.5 V with laser techniques, while short circuit current densities were typical for the substrate used, suggesting increased emitter recombination current, (39-40), (a similar problem perhaps as with trimethyl borate devices). When open circuit voltage is controlled by emitter (and bulk) leakage, it has been found to be sensitive to several emitter properties including dopant concentration and profile, junction depth and surface recombination velocity. This has been discussed in detail by Shibib and Fossum (39). However, the use of a fine grid resulted in a 20% average improvement in FF and subsequently, power efficiency. Typical sheet resistances were 150 ohms/sq., the highest seen of all molecular dopants.

Thermal annealing techniques involved only 3-step anneals. Open circuit voltages were 520-530 mV, indicating a larger junction potential for the type of implant than realized with lasers. Fill factors were also significantly improved with fine grid.

Diode Measurements

Small mesa diodes of 0.015 cm^2 area were formed from various implanted emitter regions. After recording the dark forward bias I-V curves, both n, the ideality factor, and J_o, the saturation current density were determined. Factor n is calculated using the modified Shockley equation $J = J_o (\exp(qV/nkT)-1)$ using the slope of the log I versus V curve. Quantity J_o is calculated using the previously calculated n and the value of J at 0.5V forward bias. Table V summarizes the diode data and includes data from a conventionally implanted (^{11}B, $2\times10^{15}/cm^2$, 35 keV) ruby laser annealed mesa diode of similar fabrication for comparison.

TABLE V

Mesa Diode Junction Parameters

Cell	Annealing	n-Ideality	J_o-Measured ($\times 10^{-8}$ A/cm^2)
^{31}P (#57)	1.5J/cm^2	1.19	4.32
^{31}P (#51)	1.5 J/cm^2 - 700°C/20 min.	1.27	25.20
^{31}P (#54)	3-Step	1.20	6.58
$POCl_3$-Diff (#2)	550°C	1.34	3.52
$P(OCH_3)_3$ (#111)	1.5 J/cm^2	1.38	49.30
PCl_3 (#212A)	1.5 J/cm^2	1.40	265.00
Reference 5		1.22	7.00

Quantum Efficiency Measurements

External quantum efficiency results are given in Fig. 12 for four solar cells. For the two conventional implanted ^{31}P cells the effects of annealing on the spectral response are striking. With Cell #9 (1000°C 1-step), short wavelength or blue efficiency is lacking because of probable emitter phosphorus precipitates and poorer implant damage recrystallization. It is postulated that the red response is poor due to a reduction in the minority carrier diffusion length caused by the high temperature annealing. The improved spectral response of the laser annealed cell would seem to point to improved overall crystallinity and the maintenance of bulk minority carrier lifetime.

The quantum efficiency of the BF_3 cells is degraded by their lower short circuit current values, at best 10% lower than typical values for other molecular implants. Even with this correction the blue response is inferior to the conventional implanted cells, again pointing to the very high doping densities in the emitter region for this type of cell. The BF_3 cell with laser anneal only is inferior to the same cell with a post laser anneal of 700°C. However, even with incomplete recrystallization this cell has noticeably better quantum efficiency than a conventionally implanted cell with a 1000°C thermal anneal.

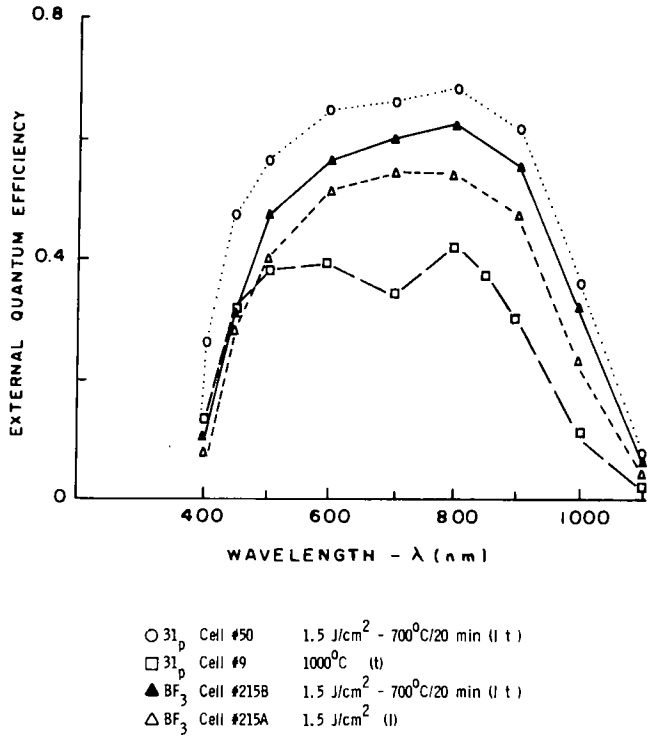

Fig. 12. External quantum efficiency measurements of ion implanted cells with various annealing techniques.

Summary and Concluding Remarks

With the use of very simple low voltage, molecular gas, glow discharge implantation without mass separation, this study has shown that non AR coated silicon pn junction solar cell power efficiencies greater than 8% (8.2% maximum, AM1) can be realized with molecular sources other than BF_3 and PF_5. In fact better performance over that of BF_3 was obtained with BCl_3, PCl_3, AsF_3 and $POCl_3$, the overall best being BCl_3. The lower relative performance of BF_3 we attribute to incomplete emitter annealing with a Q-switched ruby laser. This maximum efficiency is to be compared with solar devices made with conventional implantation (^{11}B or

^{31}P at 30 keV) or open tube diffusion with $POCl_3$ at 855°C where conversion efficiencies under identical test conditions were 9.1%. Although laser annealing was essential to obtain best performance, open circuit voltage and fill factor were the major cell limitations seen.

For similar implantation and anneal conditions, sheet resistances for annealed layers were generally directly related to the dopant species molecular weight. Source BF_3 with molecular weight of 67.8 produced emitter resistances of 30-50 ohms/sq., while $AsCl_3$ with a molecular weight of 181.27 produced resistances of 135 to 180 ohms/sq. The relationship between these implant conditions and the resulting emitter layer sheet resistance was repeatable for a given source but somewhat ambiguous in general.

Surface sputtering, dopant nonuniformity and high temperature may be a problem for the target sample with the glow discharge method. Nevertheless we have found the method to be attractive in view of its inherent low voltage and high operating currents allowing for shallow emitter layers necessary for enhanced blue photon response and implant times of as little as four minutes.

It was not the intent of this study to optimize the glow discharge implantation/laser-thermal anneal procedure but rather to perform an initial survey on molecular species that could favorably be used with this technique. Now that certain dopants have been identified (BCl_3, PCl_3, AsF_3, $POCl_3$) it is our belief that future work should be concentrated on these. The research should attempt to establish a better relationship between emitter layer formation (conditions of I, V, t and anneal) and its electrical and structural condition. Electrical analysis would include the activation percentages of implanted dopant and resulting carrier mobility. The structural analysis would primiarily consist of Rutherford backscattering for a monitor of crystalline state for the various implantations and anneals. Of course, these analyses should correlate with resulting cell performance.

Acknowledgement

The authors would like to thank several individuals for assistance at various phases of this work: Elaine Charlson, John Farmer, Jon Meese and Bill Richardson (all of University of Missouri), Rosa Young and Gerard van der Leeden (Oak Ridge National Labs), for stimulating discussions and cell performance measurements; Bob Sandfort (Monsanto) and Wayne Grubbs (Hewlett-Packard) for supplying silicon wafers; Earl Caruthers (University of Missouri) for fabricating experimental equipment; Paul Hicken and Mike Warburton (Motorola) for performing SIMS analysis; and Bill Clow (Western Electric) for performing the conventional ion implantations.

References

1. R.T. Young, R.F. Wood, J. Narayan, C.W. White and W.H. Christie, IEEE Trans. Electron Devices ED-27, 807 (1980).

2. A.R. Kirkpatrick, J.A. Minnucci and A.C. Greenwald, Proc. IEEE Photo. Spec. Conf., 14th, 820 (1980).

3. E.C. Douglas and R.V. D'Aiello, IEEE Trans. Electron Devices ED-27, 792 (1980).

4. P. Ostoja, S. Solmi and A. Zani, J. Appl. Phys. 52, 6208 (1981).

5. C.W. White, J. Narayan and R.T. Young, Laser-Solid Interactions and Laser-Processing-1978, S.D. Ferris, H.J. Leamy and J.M. Poate, eds., American Institute of Physics, New York (1979), p. 275.

6. R.T. Young, R.F. Wood, W.H. Christie and G.E. Jellison, Jr., Appl. Phys. Lett. 39, 313 (1981).

7. R.T. Young, C.W. White, J. Narayan, R.D. Westbrook, R.F. Wood, and W.H. Christie, Proc. IEEE Photo. Spec. Conf., 13th, 717 (1978).

8. D.G. Beanland, Solid-State Electron. 21, 537 (1978).

9. S. Prussin, Proc. of the Fourth International Conf. on Ion Implantation, 449 (1975).

10. B.A. MacIver and E. Greenstein, J. Electrochem. Soc. 124, 273 (1977).

11. H. Müller, H. Ryssel and I. Ruge, Proc. of the Second International Conf. on Ion Implantation in Semiconductors, 85 (1971).

12. R.G. Wilson, Low-energy Ion Beams 1977, K.G. Stephens, I.H. Wilson, and J.L. Moruzzi, eds., The Institute of Physics, London (1978).

13. R. Wichner and E.J. Charlson, J. Electron. Mater. 5, 513 (1976).

14. J.P. Ponpon and P. Siffert, Proc. IEEE Photo. Spec. Conf., 11th, 342 (1975).

15. J.C. Muller, A. and J.J. Grob, R. Stuck and P. Siffert, Proc. IEEE Photo. Spec. Conf., 13th, 711 (1978).

16. J.G. McCallum, G.I. Robertson, A.F. Rodde, B. Weissman and N. Williams, J. Vac. Sci. Technol. 15, 1067 (1978).

17. B. Chapman, Glow Discharge Processes, John Wiley and Sons, New York (1980).

18. L.T. Lamont, Jr., private communication.

19. P.D. Parry, J. Vac. Sci. Technol. 14, 622 (1976).

20. L.T. Lamont, Jr., Solid State Technol. 22, 107 (1979).

21. G. Dearnaley, J.H. Freeman, R.S. Nelson and J. Stephen, Ion Implantation, North-Holland Publishing Co., Amsterdam (1973).

22. L.J. Chen and I.W. Wu, J. Appl. Phys. 52, 3310 (1981).

23. G. Carter, J.S. Colligon and J.H. Leck, Proc. Phys. Soc. 79, 299 (1962).

24. E.F. Krimmel and H. Pfleiderer, Radiat. Effects 19, 83 (1973).

25. J.H. Freeman, Applications of Ion Beams to Materials 1975, G. Carter, J.S. Colligon and W.A. Grant, eds., The Institute of Physics, London (1975), p. 340.

26. F.M. Smits, Bell System Tech. J. 37, 711 (1958).

27. H.J. Leamy, G.A. Rozgonyi, T.T. Sheng and G.K. Celler, Appl. Phys. Lett. 32, 535 (1978).

28. G.N. Maracas, G.L. Harris, C.A. Lee and R.A. McFarlane, Appl. Phys. Lett. 33, 453 (1978).

29. J. Narayan in Inst. Phys. Conf. Series No. 60, Microscopy of Semiconducting Materials 1981, A.G. Cullis, D.C. Joy, Eds., Inst. of Physics, London (1981), p. 101.

30. G.J. van Gurp, G.E.J. Eggermont, Y. Tamminga, W.T. Stacy and J.R.M. Gijsbers, Appl. Phys. Lett. 35, 273 (1979).

31. R.W. Rostron, IEEE Trans. Electron Devices ED-19, 1024 (1972).

32. A.W. Fisher and J.A. Amick, J. Electrochem. Soc. 113, 1054 (1966).

33. J. Mandelkorn and J.H. Lamneck, Jr., Proc. IEEE Photo. Spec. Conf., 9th, 66 (1972).

34. J.L. Benton, L.C. Kimerling, G.L. Miller, D.A.H. Robison and G.K. Celler, Laser and Electron Beam Processing of Materials, C.W. White and P.S. Pearcy, eds., Academic Press, New York (1980), pp. 430-434.

35. A. Mesli, J.C. Muller, D. Salles and P. Siffert, Appl. Phys. Lett. 39, 159 (1981).

36. J. Lindhard, M. Scharff and H.E.Schiøtt, Kgl. Danske Videnskab Selskab. Mat. Fys Medd. 33, 14 (1963).

37. E. Fogarassy, R. Stuck, J.C. Muller, A. and J.J. Grob, P. Siffert, Y. Salles and D. Diguet, Proc. European Communities Photo. Solar Energy Conf., 2nd, 768 (1979).

38. D.G. Beanland, W. Temple and D.J. Chivers, Solid-State Electron. 21, 357 (1978).

39. M.A. Shibib and J.G. Fossum, J. Appl. Phys. 52, 1072 (1981).

40. R.T. Young, R.F. Wood and W.H. Christie, J. Appl. Phys. 53, 1178 (1982).